

# UNDERSTANDING AND RESOLVING SINGULARITIES IN 3D DIRICHLET BOUNDARY PROBLEMS

DAVID LEVIN

ABSTRACT. We introduce a two-phase approximation method designed to resolve singularities in three-dimensional harmonic Dirichlet problems. The approach utilizes the classical Green's function representation, decomposing the function into its singular and regular components.

The singular phase employs Green's formula with the singular part, for which we show that it induces the necessary singularities in the solution. The regular phase then introduces a smooth correction to recover the remaining regular part of the solution. The construction employs high-order quadrature rules in the first phase, followed by collocation with a suitable harmonic basis in the second.

## 1. INTRODUCTION

### PROBLEM SETUP

Let  $\Omega \subset \mathbb{R}^3$  be a bounded domain with boundary  $\partial\Omega$ , and consider the Dirichlet problem:

$$\begin{cases} \Delta u = 0, & \text{in } \Omega, \\ u = f, & \text{on } \partial\Omega. \end{cases}$$

The boundary  $\partial\Omega$  may be smooth or non-smooth, and the boundary data  $f$  may be continuous on  $\partial\Omega$ , piecewise continuous, or in  $L^2(\partial\Omega)$ .

A weak solution  $u \in H^1(\Omega)$  exists under mild assumptions on the boundary data (e.g.,  $f \in L^2(\partial\Omega)$ ), and the solution is harmonic; hence, it is infinitely differentiable in the interior of  $\Omega$ . However, the solution may exhibit singular behavior near geometric singularities of the domain, such as the corners of  $\partial\Omega$ , as well as near discontinuities in the boundary data  $f$ . In particular, the gradient  $\nabla u$  may become unbounded in the vicinity of these singularities.

One of the most widely used practical methods for solving elliptic boundary value problems is the Finite Element Method (FEM); see Babuška [1]. However, in problems governed by the Laplace and Poisson equations, the spatial derivatives of the potential field may become unbounded near corners and edges of the domain. As a result, conventional finite elements often fail to capture the solution accurately in the vicinity of such singularities. This limitation has motivated significant research into the development and implementation of specialized singular elements for two-dimensional finite element analysis, specifically designed to resolve corner

<sup>1</sup>David Levin, School of Mathematical Sciences, Tel-Aviv University, Israel

and edge singularities in potential problems: see, for example, [6, 11, 12, 15, 16]. However, in contrast to the two-dimensional case, the explicit characterization of singularities in solutions to the three-dimensional harmonic problem near corners and edges remains incomplete.

In the two-dimensional setting, a corrected collocation approach for treating corner singularities was proposed in [13]. The method is tailored to geometric configurations that admit a singular-regular decomposition of the corresponding Green's function. The extension of this approach to higher dimensions has, to the best of our knowledge, remained unresolved. The purpose of the present paper is to address this problem.

The results presented here extend the methodology of [13] to three dimensions. While the applicability of the method is still confined to certain geometric structures, it already covers important examples, including cubes and cylinders. Furthermore, the analysis developed in this work provides a framework for understanding the singular behavior of solutions in more general geometries.

The paper is organized as follows. In Section 2 we recall Green's identity and review explicit representations of the Dirichlet Green's function in geometries of interest, including the half-space, the unit cube, and cylindrical domains. These examples motivate the singular-regular decomposition employed throughout the paper. In Section 3 we formulate the S-R method in a general setting, establish the decomposition of the solution into singular and harmonic components, and describe the resulting two-phase approximation procedure. Particular attention is given to the implementation for the unit cube, including the computation of the singular integral contribution, the construction of harmonic approximants via both polynomial interpolation and the method of fundamental solutions, and the treatment of nearly singular boundary integrals. Section 4 presents numerical experiments that assess stability, conditioning, and accuracy of the proposed method, with emphasis on corner-induced singularities and high-order evaluation of the solution near the boundary.

## 2. PRELIMINARIES - GREEN'S IDENTITY AND GREEN'S FUNCTION

Let  $\Omega \subset \mathbb{R}^3$  be a bounded domain with sufficiently smooth boundary  $\partial\Omega$ . We consider the harmonic Dirichlet problem

$$\begin{cases} -\Delta u(x) = 0, & x \in \Omega, \\ u(x) = f(x), & x \in \partial\Omega. \end{cases} \quad (2.1)$$

Given boundary data  $f$  on  $\partial\Omega$ , the objective is to determine a function  $u : \bar{\Omega} \rightarrow \mathbb{R}$  that is harmonic in  $\Omega$  and satisfies the prescribed boundary values. Under standard assumptions on  $f$  (for example,  $f \in L^2(\partial\Omega)$ ), the problem admits a weak solution  $u \in H^1(\Omega)$ , which is smooth in the interior of  $\Omega$ .

In 1828, George Green presented his second integral identity:

$$\int_{\Omega} (u \Delta v - v \Delta u) dV = \int_{\partial\Omega} \left( u \frac{\partial v}{\partial n} - v \frac{\partial u}{\partial n} \right) dS.$$

Building on this identity, Green introduced what is now known as Green's function, providing an explicit integral representation for solutions of Laplace's equation.

Let  $\Omega \subset \mathbb{R}^3$  be a closed domain with a piecewise smooth boundary  $\partial\Omega$ . The Green's function  $G(x, y)$  for the Laplace operator in  $\Omega$  is defined as the function satisfying

$$\begin{cases} \Delta_y G(x, y) = -\delta(x - y), & y \in \Omega, \\ G(x, y) = 0, & y \in \partial\Omega. \end{cases} \quad (2.2)$$

Here  $\delta$  denotes the Dirac delta distribution, and  $\Delta_y$  is the Laplacian with respect to the variable  $y$ .

Given boundary data  $u = f$  on  $\partial\Omega$ , the harmonic Dirichlet problem

$$\Delta u = 0 \quad \text{in } \Omega, \quad u = f \quad \text{on } \partial\Omega \quad (2.3)$$

has the solution representation [10]

$$u(x) = \int_{\partial\Omega} \frac{\partial G}{\partial n_y}(x, y) f(y) ds_y, \quad x \in \Omega, \quad (2.4)$$

where  $\frac{\partial G}{\partial n_y}$  denotes differentiation with respect to the outward unit normal at  $y \in \partial\Omega$ .

*The Green's function method reduces solving the PDE to computing integrals over the domain boundary. It naturally incorporates the boundary data and provides an elegant integral representation for the solution.*

The fundamental solution of the Laplace operator in  $\mathbb{R}^3$  is

$$G(x, y) = \frac{1}{4\pi|x - y|} \equiv \Phi(|x - y|), \quad x \neq y. \quad (2.5)$$

The point  $y$  is called the *source point*, and the function  $\Phi(|x - y|)$  is referred to as the *source function*.

### 2.1. Green's Function for the Half-Space $x_3 \geq 0$ .

Let  $x = (x_1, x_2, x_3) \in \Omega$  and  $y = (y_1, y_2, y_3) \in \Omega$  be a source point. The Green's function for Laplace's equation in the upper half-space with Dirichlet boundary condition is:

$$G(x, y) = \frac{1}{4\pi} \left( \frac{1}{|x - y|} - \frac{1}{|x - y^*|} \right),$$

where  $y^* = (y_1, y_2, -y_3)$  is the reflection of  $y$  across the plane  $x_3 = 0$ . This ensures:

- $G(x, y) = 0$  for  $x \in \partial\Omega$ ,

- $\Delta_x G(x, y) = -\delta(x - y)$  in  $\Omega$ .

Since  $\Delta u = 0$ , the representation becomes:

$$u(y) = - \int_{\partial\Omega} \frac{\partial G}{\partial n_x}(x, y) g(x) dS(x),$$

where  $n_x$  is the outward normal at  $x \in \partial\Omega$ . Since  $\partial\Omega$  is the plane  $x_3 = 0$ , the outward normal is  $n_x = (0, 0, -1)$ ,

so:

$$\frac{\partial G}{\partial n_x} = -\frac{\partial G}{\partial x_3}.$$

**Normal Derivative of Green's Function.** Differentiating  $G(x, y)$  with respect to  $x_3$  at  $x_3 = 0$ , we obtain:

$$-\frac{\partial G}{\partial x_3}(x, y) \Big|_{x_3=0} = \frac{y_3}{2\pi (|x' - y'|^2 + y_3^2)^{3/2}}, \quad (2.6)$$

where  $x' = (x_1, x_2)$  and  $y' = (y_1, y_2)$ . This is known as the **Poisson kernel** for the 3D half-space:

$$P(x', y) = \frac{y_3}{\pi (|x' - y'|^2 + y_3^2)^{3/2}}.$$

Substituting into the representation formula:

$$u(y) = \int_{\mathbb{R}^2} P(x', y) g(x') dx'.$$

As  $y = (y', y_3) \rightarrow (x'_0, 0) \in \partial\Omega$ , the Poisson kernel  $P(x', y)$  becomes sharply peaked around  $x' = x'_0$ , and tends to a delta function:

$$\lim_{y_3 \rightarrow 0^+} u(y', y_3) = g(y').$$

Therefore, the function  $u(y)$  defined by Green's representation (or equivalently, the Poisson integral) satisfies the Dirichlet boundary condition:

$$\lim_{y \rightarrow x_0 \in \partial\Omega} u(y) = g(x_0).$$

This confirms that the Green's formula solution matches the prescribed boundary values on  $\partial\Omega$ .

## 2.2. The unit cube.

For  $\Omega = [0, 1]^3$ , the Dirichlet Green's function can be expressed using the method of images as a tri-infinite lattice sum of free-space sources placed at the reflected image points.

$$G^\square(x, y) = \sum_{n \in \mathbb{Z}^3} \sum_{m \in \{0,1\}^3} (-1)^{m_1+m_2+m_3} \Phi(x - y_{n,m}), \quad (2.7)$$

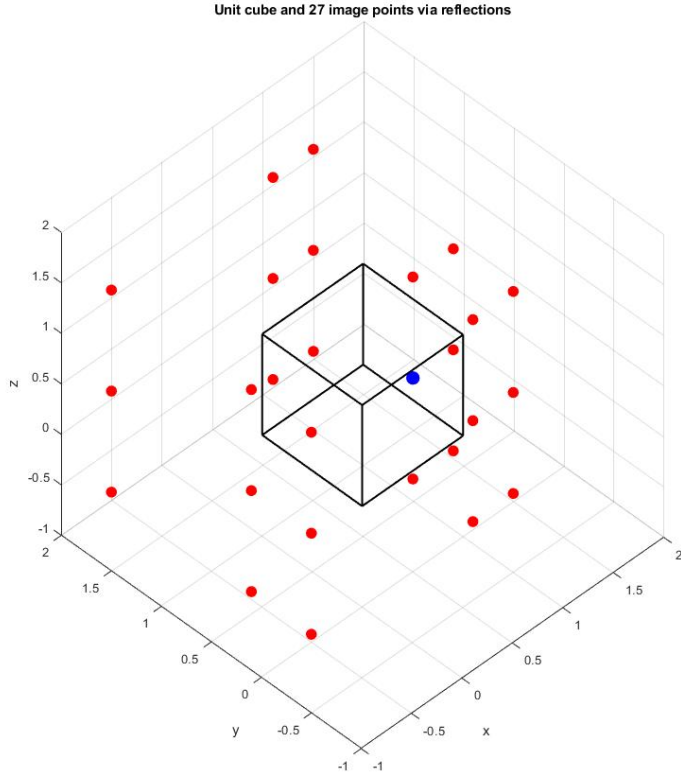


FIGURE 1. The unit cube; The source point in blue plus 26 triple reflections in red.

where

$$\Phi(z) = \frac{1}{4\pi|z|}, \quad y_{n,m} = ((-1)^{m_1}y_1 + 2n_1, (-1)^{m_2}y_2 + 2n_2, (-1)^{m_3}y_3 + 2n_3),$$

and

$$n = (n_1, n_2, n_3) \in \mathbb{Z}^3, \quad m = (m_1, m_2, m_3) \in \{0, 1\}^3.$$

This yields the Dirichlet Green's function in the unit cube  $[0, 1]^3$ . The series is conditionally convergent.

We denote by  $G_{27}$  the 27 source functions that are closest to the cube:

$$G_{27}^{\square}(x, y) = \sum_{i,j,k=-1}^1 \sum_{m_1, m_2, m_3=0}^1 (-1)^{m_1+m_2+m_3} \Phi\left(x - y_{m_1, m_2, m_3}^{(i,j,k)}\right), \quad (2.8)$$

$$y_{m_1, m_2, m_3}^{(i,j,k)} = ((-1)^{m_1}y_1 + 2i, (-1)^{m_2}y_2 + 2j, (-1)^{m_3}y_3 + 2k).$$

### 2.3. The cylinder.

Let  $x = (r, \theta, z)$ ,  $y = (r', \theta', z')$ , with  $0 \leq r, r' < a$ . Let  $\alpha_{n,m}$  be the  $m$ th positive zero of  $J_n$ . The Dirichlet Green's function in the infinite cylinder is

$$G(x, y) = \frac{1}{2\pi} \sum_{n=-\infty}^{\infty} e^{in(\theta-\theta')} \sum_{m=1}^{\infty} \frac{J_n\left(\frac{\alpha_{n,m}r}{a}\right) J_n\left(\frac{\alpha_{n,m}r'}{a}\right)}{\alpha_{n,m} a [J_{n+1}(\alpha_{n,m})]^2} e^{-(\alpha_{n,m}/a)|z-z'|}. \quad (2.9)$$

It satisfies  $G = 0$  for  $r = a$  and has the free-space singularity  $G(x, y) \sim \frac{1}{4\pi|x-y|}$  as  $x \rightarrow y$ .

#### 2.4. The finite cylinder.

Let  $G_0(x, y)$  denote the Dirichlet Green's function of the infinite cylinder of radius 1. For  $y = (r', \theta', y_z) \in \{r' < 1, 0 \leq y_z \leq 1\}$ , define the axial images

$$y^{(k)} = (r', \theta', y_z^{(k)}), \quad y_z^{(k)} = (-1)^k y_z + 2k, \quad k \in \mathbb{Z}.$$

The **Dirichlet Green's function** for the finite unit cylinder  $\Omega = \{(r, \theta, z) : 0 \leq r < 1, 0 \leq z \leq 1\}$ , vanishing on the boundaries  $r = 1$ ,  $z = 0$ , and  $z = 1$ , is given by the image series

$$G^\circ(x, y) = \sum_{k \in \mathbb{Z}} (-1)^k G_0(r, \theta, z; r', \theta', y_z^{(k)}),$$

where  $y_z^{(k)}$  denotes the reflected  $z$ -coordinates. For later use, we introduce the **three-term image expansion**:

$$G_3^\circ(x; r', \theta', z') = G_0(x; r', \theta', z') - G_0(x; r', \theta', -z') - G_0(x; r', \theta', 2 - z'). \quad (2.10)$$

#### 2.5. Reviewing the Corrected Collocation Method in 2D.

The paper [13] introduces a method to improve collocation approximations for the harmonic Dirichlet problem by addressing the singular behavior of the Green's function.

Standard collocation often fails to produce efficient global approximations because the distribution of "best" collocation points is strongly correlated with the singularities of the Green's function, which vary depending on the specific point being evaluated.

The paper [13] suggests overcoming this by:

- **Singular-Regular Decomposition:** Splitting the normal derivative of the Green's function ( $G$ ) into a **singular part** ( $S$ ) and a **regular part** ( $R$ ).
- **Correction Term:** Adding an integral correction term to the initial collocation approximation. This term utilizes the singular part  $S$  to "remove" the singular effect.

- **Quadrature Selection:** Choosing collocation points as the abscissae of a best quadrature formula for the regular part  $R$ . This ensures that the approximation is efficient across the entire domain, not just at a single point.

The paper proposes a further improvement by approximating the remaining error in the corrected solution. Since the correction term cancels the oscillatory behavior of the initial error, this "remainder" can be effectively modeled using another round of collocation with harmonic polynomials.

Let  $\Omega \subset \mathbb{R}^2$  be a bounded domain with a smooth boundary  $\Gamma$ , and let  $u$  be the harmonic function satisfying

$$\Delta u = 0 \quad \text{in } \Omega, \quad u = f \quad \text{on } \Gamma.$$

The procedure in [13] begins with a collocation approximation of the form

$$u_h(x, y) = \sum_{j=1}^N a_j \phi_j(x, y),$$

where  $\{\phi_j\}$  are smooth trial functions (e.g., harmonic polynomials). The coefficients  $a_j$  are determined by imposing boundary conditions at collocation points  $\{(x_i, y_i)\}_{i=1}^N \subset \Gamma$ :

$$u_h(x_i, y_i) = f(x_i, y_i).$$

The main idea in [13] is to add a *correction term* using the singular part  $S$  of the Green's function  $G$ . The corrected approximation is defined as

$$u_h^c(x_0, y_0) = u_h(x_0, y_0) + \int_{\partial\Omega} \frac{\partial S}{\partial n}(x_0, y_0; x, y) \left( f(x, y) - \sum_{j=1}^N \alpha_j \phi_j(x, y) \right) ds.$$

In [13] it was demonstrated that, for a unit square with jump discontinuities at the corners, the corrected collocation method reduces the error from 0.5 to 0.00125, using only 16 collocation points.

The present paper is not just an extension of [13] to the 3D case. It also makes use of the decomposition of the Green's function into the singular and regular parts, but in a substantially different way.

## 2.6. Challenges in Solving the Unit Cube Problem.

In many practical applications, solving the Laplace equation within a cubic domain subject to Dirichlet boundary conditions is a fundamental task.

Often, the prescribed boundary data are discontinuous, which induces singular behavior in the solution near the boundaries, specifically in the vicinity of edges and corners.

From a numerical perspective, classical discretization techniques such as the Finite Element Method (FEM) can approximate these solutions. However, the presence of these singularities often leads to a deterioration in convergence rates. Consequently, achieving high-precision results typically requires intensive local mesh refinement or the implementation of specialized singular-enrichment techniques. Capturing the correct singularities at the corners and edges of the cube is challenging and often leads to reduced accuracy if standard basis functions are used. Special techniques, such as mesh refinement near singularities or enriched basis functions, are needed to maintain accuracy without excessive computational effort.

Solving the Dirichlet problem for the Laplace equation in a cube, or more generally in a polyhedral domain, entails distinctive difficulties. Even for smooth boundary data, the solution may exhibit singular behavior near edges and corners.

The paper [15] investigates the high-resolution analysis of such singularities in three dimensions using the neBEM solver. The works [2, 6] study the Sobolev regularity of harmonic functions in polyhedral domains, including the cube, and show that the gradient of the solution typically becomes unbounded in the vicinity of edges and vertices. The paper [16] develops computational techniques, based on singular boundary elements, that are tailored to capture and resolve these corner and edge effects.

We conclude that, in a three-dimensional cube, the geometry itself may generate singularities, even when the prescribed boundary data are smooth. These singularities do not occur in the solution  $u$ , which remains continuous, but rather in its derivatives, especially near edges and corners.

The present paper is not merely a three-dimensional extension of [13]. Although it also relies on a decomposition of the Green's function into singular and regular components, the decomposition is exploited here in a fundamentally different manner. In the following section, we introduce a two-phase method for the high-order evaluation of the solution. The resulting approach remains stable and accurate even in the presence of sharp singularities.

### 3. THE S–R METHOD

#### 3.1. Singular–Regular Decomposition of the Green's Function.

In certain cases, the Green's function is known explicitly, allowing the solution to the harmonic Dirichlet problem to be computed via boundary integrals using the representation formula (2.4). However, for many domains, most notably the unit cube, the Green's function is expressed only as a formal series, making its practical evaluation non-trivial. In the following sections, we adopt the unit cube as our primary model setting.

We assume that the Green's function associated with a domain  $\Omega$  admits the decomposition

$$G(x, y) = S(x, y) + R(x, y), \tag{3.1}$$

where  $S$  represents the singular part of  $G$  and  $R$  its regular part. In what follows, we further assume that  $S$  is available and can be computed with relative ease, whereas  $R$  is not.

**Definition 3.1.** *Let  $U \subset \mathbb{R}^n$  be an open domain and  $\Omega \subset U$  be a closed domain. We say that  $R(x, y)$  is **regular of order**  $m$  on  $U \times \Omega$  if, for every multi-index  $\alpha$  with  $|\alpha| \leq m$ , the partial derivative  $D_x^\alpha R(x, y)$  exists and is bounded on  $U \times \Omega$ .*

**Remark 3.2.** *Note that the definition implies that, for each fixed  $y \in \Omega$ , the derivatives  $D_x^\alpha R(x, y)$  exist and are bounded for all  $x \in U$ .*

A two-dimensional instance of the decomposition (3.1), together with its practical use, is given in [13]. Here, we take as our main example the Green's function for the unit cube, introduced above in (2.7). We decompose  $G^\square$  into a singular-regular form as

$$G^\square(x, y) = G_{27}^\square(x, y) + R_{27}^\square(x, y), \quad (3.2)$$

where  $G_{27}^\square$  is the partial sum defined in (2.8), and  $R_{27}^\square$  is the remainder of the tri-infinite expansion (2.7). For any  $y \in [0, 1]^3$ , the remainder  $R_{27}^\square(x, y)$  is harmonic in  $x$  throughout the enlarged domain  $(-1, 2)^3$  and thus constitutes the **regular part** of  $G^\square$ . The partial sum  $G_{27}^\square(x, y)$  serves as the **singular part**; it contains the primary singularity within the unit cube and 26 additional singularities in  $(-1, 2)^3$  arising from triple reflections.

Similarly, the Green's function for the unit cylinder  $\Omega = \{(r, \theta, z) : 0 \leq r < 1, 0 \leq z \leq 1\}$  admits the decomposition

$$G^\circ(x, y) = G_3^\circ(x, y) + R_3^\circ(x, y), \quad (3.3)$$

where the remainder  $R_3^\circ$  is harmonic in the extended domain  $-1 < z < 2$ .

### 3.2. The Singular-Regular (S–R) approach.

Assuming the Green's function admits the decomposition (3.1), the solution of the Dirichlet problem in  $\Omega$  is written as

$$u(x) = H_S(x) + H_R(x), \quad x \in \Omega. \quad (3.4)$$

where

$$H_R(x) \equiv \int_{\partial\Omega} \frac{\partial R}{\partial n_y}(x, y) f(y) ds_y. \quad (3.5)$$

and

$$H_S(x) \equiv \int_{\partial\Omega} \frac{\partial S}{\partial n_y}(x, y) f(y) ds_y. \quad (3.6)$$

**Assumption 3.3.** *Motivated by the cases of the unit cube and the unit cylinder, we assume that for any fixed  $y \in \Omega$ , the regular part  $R(\cdot, y)$  is harmonic in an open domain  $U$  such that  $\Omega \subset U$ .*

The following elementary observations constitute the foundation of the proposed S–R approach.

**Corollary 3.4.** *In view of Assumption 3.3, the solution admits the decomposition (3.4) where*

- (A)  $H_R$  is harmonic in  $U$ .
- (B) All singular behavior of the solution  $u$  is contained in  $H_S$ .

### 3.3. The approximation procedure.

Based on Corollary 3.4, we propose the following approximation procedure.

- (1) Select  $N$  points  $\{x_i\}_{i=1}^N$  distributed over  $\partial\Omega$ .
- (2) Evaluate

$$H_S(x_i) = \int_{\partial\Omega} \frac{\partial S}{\partial n_y}(x_i, y) f(y) ds_y, \quad i = 1, \dots, N, \quad (3.7)$$

using a suitable quadrature rule, denote the resulting approximations by  $\tilde{H}_S(x_i)$ .

- (3) Compute

$$\tilde{H}_R(x_i) = u(x_i) - \tilde{H}_S(x_i), \quad i = 1, \dots, N. \quad (3.8)$$

- (4) Construct a harmonic approximation  $P_N$  of  $H_R$  from the data  $\{\tilde{H}_R(x_i)\}_{i=1}^N$ .
- (5) For any given  $x \in \Omega$ , approximate  $H_S(x)$  by  $\tilde{H}_S(x)$  using a suitable quadrature rule.
- (6) Define the approximation  $u_N$  to  $u$  at  $x \in \Omega$  by

$$u_N(x) = \tilde{H}_S(x) + P_N(x). \quad (3.9)$$

**Observation 3.5.** *Once the global harmonic approximation of  $H_R$  is available, the evaluation of  $u$  at any prescribed point  $x$  reduces to a separate and independent computation.*

**Observation 3.6.** *The approximation  $u_N$  in (3.9) consists of a harmonic approximation  $P_N$  of  $H_R$  and a component  $\tilde{H}_S$ , which is generally non-harmonic. Indeed,  $\tilde{H}_S(x)$  is typically not harmonic in  $x$ , since the quadrature rule used in step (5) above depends on the evaluation point  $x$ .*

In the sequel, we examine the individual steps of the approximation procedure, with particular emphasis on the unit cube.

### 3.4. Theoretical and implementation details for the unit cube.

For the unit cube, we recall that the singular part is  $S = G_{\square}^{27}$ , as defined in (2.8), and the corresponding regular part is  $R = R_{\square}^{27}$ , see (3.2). As shown below,  $R(\cdot, y)$  is harmonic in the enlarged domain  $(-1, 2)^3$ . We now prove that the associated regular component of the solution is likewise harmonic in  $(-1, 2)^3$ .

**Proposition 3.7.** *Let  $\Omega = [0, 1]^3$  and consider the decomposition (3.2), where  $G_\square$  is given by the lattice representation (2.7) and  $G_\square^{27}$  by the truncated sum (2.8). Then, for every  $y \in \Omega$ , the remainder  $R_\square^{27}(\cdot, y)$  is harmonic in the enlarged domain  $(-1, 2)^3$ . Consequently, the function*

$$H_R(x) = \int_{\partial\Omega} \frac{\partial R_\square^{27}}{\partial n_y}(x, y) f(y) dS_y,$$

*defined in (3.5), is harmonic in  $(-1, 2)^3$ .*

*Proof.* By (2.7), the Green's function is represented as a lattice sum of free-space source functions  $\Phi(x - y_{n,m})$ , while (2.8) retains only those terms with  $n \in \{-1, 0, 1\}^3$ . Hence, in the decomposition (3.2), the remainder  $R_\square^{27}$  consists precisely of those image terms with  $n \notin \{-1, 0, 1\}^3$ . For any  $y \in [0, 1]^3$ , such image points  $y_{n,m}$  lie outside the box  $(-1, 2)^3$ . Therefore, each term  $x \mapsto \Phi(x - y_{n,m})$  is harmonic throughout  $(-1, 2)^3$ . On compact subsets of  $(-1, 2)^3$ , the series defining  $R_\square^{27}(\cdot, y)$  admits termwise differentiation with respect to  $x$  (for instance, via uniform convergence of the second-derivative series), and thus  $\Delta_x R_\square^{27}(x, y) = 0$  in  $(-1, 2)^3$ . Differentiation with respect to  $y$  does not affect harmonicity in  $x$ , and hence  $\partial R_\square^{27}/\partial n_y(\cdot, y)$  is harmonic in  $x$  on  $(-1, 2)^3$ . Finally, the representation (3.5) shows that  $H_R$  is an integral of harmonic functions with respect to  $y$ , and is therefore harmonic in  $(-1, 2)^3$ .  $\square$

#### 3.4.1. Computing $\tilde{H}_R$ on $\partial\Omega$ .

We begin with Step (2), namely the computation of  $\tilde{H}_S(x_i)$  for  $x_i \in \partial\Omega$ .

As an illustrative example, consider a point  $x_i$  located on the upper face of the cube, namely  $z = 1$ . All source points in (2.8) that lie in the plane  $z = 1$  contribute exactly the value  $f(x_i)$  to  $H_S(x_i)$ . This follows from the analysis presented in Section 2.1. The remaining nine reflection points lie in the plane  $z = -1$ . Consequently, the corresponding normal derivatives are regular along  $\partial\Omega$ , and their contribution to the integral in (3.7) can therefore be evaluated to any prescribed accuracy using standard quadrature rules. By (3.8), the resulting quantity provides the desired approximation of  $H_R$ .

#### 3.4.2. Choosing the collocation points.

The choice of the points  $\{x_i\}_{i=1}^N$  in Step (1) has a direct impact on the quality of the harmonic interpolant  $P_N$  constructed in Step (4). We examined two alternatives. The first employs points taken from a uniform grid on each face of the cube, whereas the second uses a tensor-product grid of Gaussian points. Although both choices produced approximations of comparable accuracy, the uniform distribution yielded a markedly better conditioned interpolation matrix. This improvement in conditioning translated into enhanced numerical stability of the overall procedure.

Assuming  $N = 6n^2$ , we distribute  $n^2$  points on each face of the cube. For instance, for the face on  $z = 0$ , the uniform placement is given by  $((2i - 1)/2n, (2j - 1)/2n, 0)$ ,  $i, j = 1, \dots, n$ . The remaining faces are treated analogously.

### 3.4.3. The harmonic approximation $P_N$ .

Assume that the values  $\{\tilde{H}_R(x_i)\}_{i=1}^N$  are computed with an approximation error of order  $\varepsilon$ . Our goal is to construct a harmonic approximation  $P_N$  to  $H_R$  based on this data. We investigated two alternative approximations:  $P_N^I$ , obtained by harmonic polynomial interpolation, and  $P_N^{II}$ , constructed via the Method of Fundamental Solutions. We evaluated their performance in terms of accuracy and numerical stability.

#### The approximation $P_N^I$ :

A natural first candidate is to construct the approximation by interpolation with harmonic polynomials. In this approach, we rely on the following classical approximation result [17, 7].

Let  $\Omega$  be a bounded domain in  $\mathbb{R}^3$  (e.g., the unit cube centered at the origin). Assume that  $u$  is harmonic in an open neighborhood containing a ball  $B_R(0)$  that strictly contains  $\Omega$ . For the unit cube centered at the origin,

$$\Omega \subset B_\rho(0), \quad \rho = \frac{\sqrt{3}}{2}.$$

In our case, since  $H_R$  is harmonic in  $(-1, 2)^3$ , after translating the unit cube to be centered at the origin, the function remains harmonic in a neighborhood containing a ball of radius  $R = 3/2$ .

Expand  $u$  in solid spherical harmonics about the origin:

$$u(x) = \sum_{\ell=0}^{\infty} \sum_{m=-\ell}^{\ell} a_{\ell m} r^\ell Y_\ell^m(\theta, \phi), \quad r = |x|.$$

Let  $Q_N$  denote the truncation of this expansion to  $\ell \leq N$ , which is a harmonic polynomial of degree  $N$ . Then, for any  $0 < \rho < R$ ,

$$\|u - Q_N\|_{L^\infty(B_\rho(0))} \leq C(u, R) \left(\frac{\rho}{R}\right)^{N+1}.$$

Thus, the approximation error decays geometrically in  $N$ . The constant  $C(u, R)$  depends on an upper bound of  $u$  on  $B_R(0)$ . By the maximum principle, as the difference  $u - Q_N$  is itself harmonic, the maximum error on the interior is bounded by its values on the boundary.

In the present setting, we do not employ a spherical harmonic expansion. Instead, we construct a harmonic polynomial approximant of  $H_R$  by interpolating the approximate data  $\{\tilde{H}_R(x_i)\}_{i=1}^N$ , and we denote it as  $P_N^I$ . If  $H_R$  extends harmonically to a neighborhood strictly larger than  $\Omega$ , its polynomial approximations exhibit a geometric rate of convergence. Provided that the interpolation procedure is stable and that the data  $\tilde{H}_R(x_i)$

Cube face collocation points (colored by  $u$  values), and source points (circles)

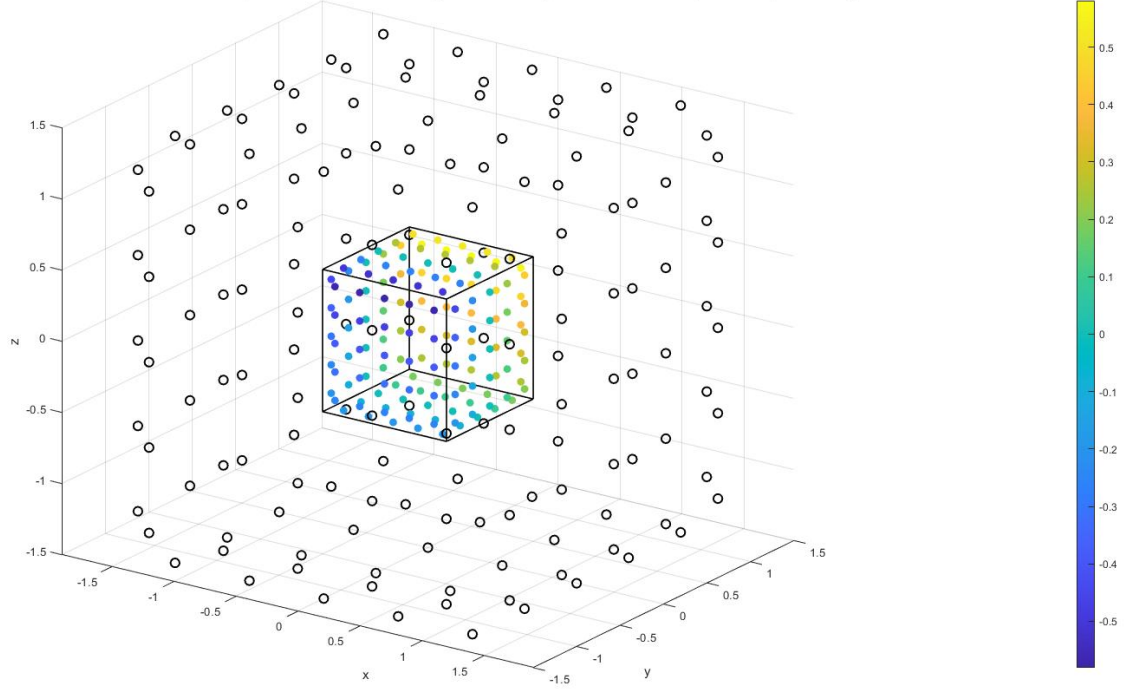


FIGURE 2. The figure shows the 150 interpolation points on the cube’s faces, colored by their sampled values, along with the corresponding source points (marked by circles) used in the interpolation basis.

approximate  $H_R(x_i)$  with sufficiently high order, the resulting interpolant  $P_N^I$  retains the same geometric rate of convergence, up to the additional error introduced by the data approximation.

**The approximation  $P_N^{II}$ :**

We further investigated an alternative interpolation strategy for approximating  $H_R$ . In this approach, the harmonic approximant is represented as a superposition of source functions. For clarity, we describe the method in the case of the unit cube centered at the origin,  $[-0.5, 0.5]^3$ . Assume that the values of a harmonic function  $u$  are given at points  $\{x_i\}_{i=1}^N$ , distributed on the faces of the cube. Define a set of source points,

$$p_i = \alpha x_i, \quad i = 1, \dots, N. \quad \alpha > 1. \tag{3.10}$$

Figure 2 illustrates a representative configuration of 150 collocation points on the faces of the cube and their associated 150 source points, with  $\alpha = 3$ .

We seek an approximation  $P_N^{II}$  of the form

$$P_N^{II}(x) = \sum_{j=1}^N c_j \Phi(|x - p_j|), \tag{3.11}$$

where  $\Phi$  is the source function defined in (2.5). The coefficients  $\{c_j\}_{j=1}^N$  are determined by enforcing the interpolation conditions

$$P_N^{\text{II}}(x_i) = \sum_{j=1}^N c_j \Phi(|x_i - p_j|), \quad i = 1, \dots, N. \quad (3.12)$$

The representation (3.11) corresponds to the classical Method of Fundamental Solutions (MFS); see, e.g., [9, 3]. At the continuous level, this ansatz can be viewed as a discrete single-layer potential with sources located outside the domain, and its validity is supported by the potential-theoretic foundations of harmonic boundary value problems. At the discrete level, the resulting interpolation matrix  $A_{ij} = \Phi(|x_i - p_j|)$  is typically invertible for generic placements of collocation and source points; however, invertibility is not guaranteed in general, and the system may become severely ill-conditioned, particularly when the sources approach the boundary.

### Comparing $P_N^{\text{I}}$ and $P_N^{\text{II}}$ :

We conducted a series of numerical experiments to identify the method most suitable for our specific application. Given a harmonic function defined on  $(-1.5, 1.5)^3$ , the experiments examined its approximation on the unit cube  $[-0.5, 0.5]^3$ . We present the results for the test case with 150 data points, distributed on a uniform grid over each of the six faces of the unit cube. The source points for  $P_N^{\text{II}}$  are defined by (3.10) with  $\alpha = 3$ . Both approximation methods were applied to the following two harmonic test functions:

$$u_1(x, y, z) = \cos(0.6x) \sin(0.8y) \exp(z),$$

$$u_2(x, y, z) = \frac{1}{\sqrt{x^2 + y^2 + (z - 1.6)^2}}.$$

We note that  $u_1$  is harmonic throughout  $\mathbb{R}^3$ , whereas  $u_2$  possesses a singularity located near the cube  $[-1.5, 1.5]^3$ .

Method	cond( $A$ )	Error in $u_1$	Error in $u_2$
$P^{\text{I}}$	$7.61 \times 10^{17}$	$8.13 \times 10^{-6}$	$8.26 \times 10^{-4}$
$P^{\text{II}}$	$4.25 \times 10^8$	$1.83 \times 10^{-5}$	$1.07 \times 10^{-5}$

TABLE 1. Condition number and approximation errors for the two test functions.

Table 1 summarizes the conditioning of the interpolation matrix and the corresponding approximation errors for the two methods. The polynomial interpolation approach  $P^{\text{I}}$  leads to an extremely ill-conditioned system ( $\text{cond}(A) \approx 7.61 \times 10^{17}$ ), yet it achieves high accuracy for the globally smooth test function  $u_1$ . However, its performance deteriorates significantly for  $u_2$ , whose nearby singularity reduces the effective radius of harmonic continuation, resulting in an error of order  $10^{-4}$ . In contrast, the method of fundamental solutions  $P^{\text{II}}$  produces a substantially better conditioned system ( $\text{cond}(A) \approx 4.25 \times 10^8$ ) and delivers consistently accurate results for both test functions, with errors of order  $10^{-5}$ . These results indicate that  $P^{\text{II}}$  is more robust, especially in the

presence of nearby singularities. When the number of data points was increased to 49 on each face of the cube, the approximation error of  $P^{\text{II}}$  for  $u_2$  decreased to  $4.15 \times 10^{-7}$ . However, this improvement came at the cost of a larger condition number, with  $\text{cond}(A) = 3.34 \times 10^{12}$ , indicating increased ill-conditioning of the system.

#### 3.4.4. Numerical error assessment for harmonic approximations of $H_R$ .

The numerical experiments above demonstrate the performance of the harmonic approximations  $P^{\text{I}}$  and  $P^{\text{II}}$  on prescribed test functions. We now turn to the more delicate task of deriving quantitative error bounds for these methods when applied to the unknown harmonic component  $H_R$ . We emphasize that such an estimate is essential for establishing a reliable global error bound for the S–R method.

Our analysis is based on the observation in Section 3.4.1 that the boundary values of  $H_R$  on the faces of the cube can be evaluated to arbitrary accuracy by means of standard quadrature schemes. For the approximation error estimation, we apply the following procedure:

- Augment the interpolation set  $\{x_i\}_{i=1}^N$  with a collection of reference points  $\{q_j\}_{j=1}^J$ , uniformly distributed over all six faces of the cube. Figure 3(A) illustrates a representative configuration with  $N = 150$ , corresponding to 25 interpolation points on each face. The interpolation points  $\{x_i\}$  are shown in red, while the reference points  $\{q_j\}$  are displayed in green.
- Compute a high-accuracy approximation of  $\tilde{H}_R \sim H_R$  at both sets of points, namely  $\{x_i\}$  and  $\{q_j\}$ .
- Using the values  $\{\tilde{H}_R(x_i)\}_{i=1}^N$ , compute the harmonic approximation  $P_N \sim H_R$  in the cube.
- Estimate the error bound for the approximation  $\tilde{H}_R$  over the cube as

$$E_R^N = 2E_{max}^N \quad (3.13)$$

where

$$E_{max}^N = \max_{j=1}^J |\tilde{H}_R(q_j) - P_N(q_j)|. \quad (3.14)$$

The error estimate (3.13) relies on the following observation:

**Observation 3.8.** *Let the interpolation points  $\{x_i\}$  be distributed on a uniform mesh of size  $h$ , and let the reference points  $\{q_j\}$  lie on a uniform mesh of size  $h/2$ , so that each  $q_j$  is located at the midpoint between two adjacent interpolation points, as illustrated in Figure 3(A). Then,*

$$\max_{x \in [0,1]^3} |\tilde{H}_R(x) - P_N(x)| = E_{max}(1 + O(h^2)). \quad (3.15)$$

*The estimate is first established for the maximum error on the faces of the cube. The global bound (3.15) then follows from the maximum principle for harmonic functions.*

### 3.4.5. A Chebyshev spectral alternative for approximating $H_R$ .

As an alternative to harmonic interpolation by polynomials or source functions, the regular component  $H_R$  may be approximated by a tensor-product Chebyshev spectral collocation method on the cube  $\Omega = [0, 1]^3$ .

Let  $x_i = \frac{1}{2}(1 + \cos(i\pi/N))$ ,  $i = 0, \dots, N$ , be the Chebyshev–Gauss–Lobatto nodes mapped to  $[0, 1]$ , and define the three-dimensional grid by the tensor product  $(x_i, y_j, z_k)$ . The Laplace equation is enforced at interior collocation points using the standard Chebyshev differentiation matrices in each coordinate direction, while the Dirichlet boundary conditions are imposed at the boundary nodes on the six faces of the cube; see, e.g., Canuto–Hussaini–Quarteroni–Zang [5].

If  $H_R$  extends harmonically to a neighborhood strictly larger than  $\Omega$ , as is the case for the cube, where  $H_R$  is harmonic in  $(-1, 2)^3$ , the Chebyshev approximation converges spectrally (i.e., exponentially) with respect to  $N$ . In order to apply this approach, the boundary values of  $H_R$  must be supplied at the  $(N + 1)^2$  Chebyshev–Gauss–Lobatto nodes on each face; as explained in Section 3.4.1, these values can be computed to any prescribed accuracy using standard quadrature rules.

We note that a detailed numerical comparison between the spectral collocation approach and the source-based approximation lies beyond the scope of the present work.

### 3.4.6. Computing $H_S$ inside $\Omega$ .

Using (2.6) together with the definition of  $H_S$  in (3.6), the evaluation of  $H_S$  reduces to the approximation of integrals of the form

$$\iint_{[0,1]^2} \frac{g(x, y)}{\left((x - a)^2 + (y - b)^2 + d^2\right)^{3/2}} dx dy, \quad (a, b) \in [0, 1]^2. \quad (3.16)$$

The main difficulty arises when  $d$  is very small. Although the integral remains finite for  $d > 0$ , the kernel becomes sharply peaked near  $(a, b)$ , and its derivatives grow rapidly in a neighbourhood of this point. Consequently, standard tensor-product quadrature rules converge slowly and may fail to deliver sufficient accuracy.

An efficient approach for treating nearly singular integrals is the self-adaptive coordinate transformation proposed by Telles [18]. This method applies a nonlinear change of variables that redistributes the quadrature nodes to cluster them near the near-singular location, thereby significantly enhancing accuracy. As a consequence, standard Gauss quadrature can still be employed, while the effective resolution is automatically increased in the region where the integrand exhibits rapid variation. This makes the method both efficient and robust for small values of  $d$ .

An alternative approach, in the same spirit but simpler to implement, is to apply standard quadrature rules on a locally refined mesh. For example, consider the integral in (3.16) with  $(a, b) = (0.2, 0.2)$  and small  $d$ . We

subdivide  $[0, 1]^2$  into nine rectangles and apply a standard tensor-product quadrature rule on each subregion, using a finer mesh in the vicinity of the near-singular point. Figure 3(B) exhibits the mesh refinement near  $(0.2, 0.2)$ .

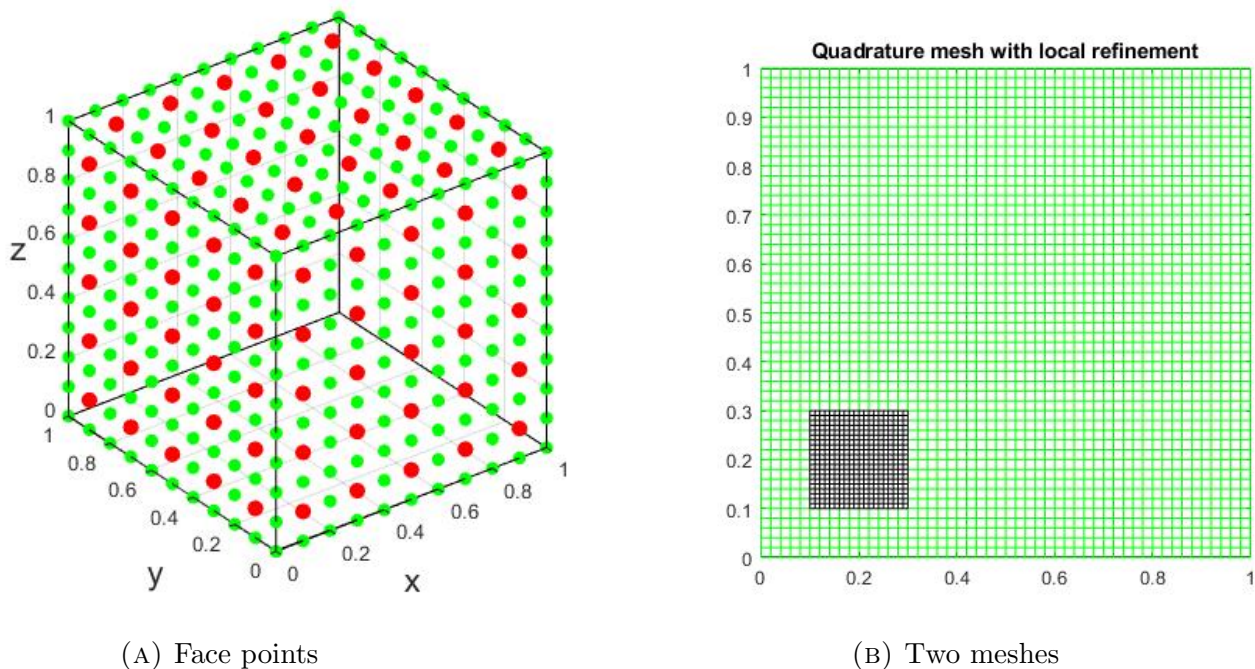


FIGURE 3

For the finite cylinder considered in Section 2.4, the singular part of the Green's function is given by (2.10), where  $G_0$  is defined by (2.9) with  $a = 1$ . We emphasize that the infinite series in (2.9) decays rapidly, owing to the exponential factor in its terms, and therefore converges very quickly in practical computations. The computation of the corresponding  $H_S$  can be performed using the same procedure described above for the unit cube.

#### 4. NUMERICAL EXPERIMENTS

We consider the Dirichlet problem for the Laplace equation in the unit cube  $\Omega = (0, 1)^3$ ,

$$\Delta u = 0 \quad \text{in } \Omega, \quad u = g \quad \text{on } \partial\Omega, \tag{4.1}$$

with piecewise constant boundary data,  $g \equiv 1$  on the upper face and  $g \equiv 0$  on all other faces. This test problem is intentionally non-smooth at the edges adjacent to the upper face. Although the solution  $u$  is continuous in  $\bar{\Omega}$ , its derivatives exhibit singular behavior near the edges and corners, which makes it a sensitive benchmark for accuracy and stability.

The test problem admits two standard physical interpretations. First, it models the electrostatic potential inside a perfectly conducting cubical cavity in which the upper face is maintained at a fixed potential  $V_0$  and the

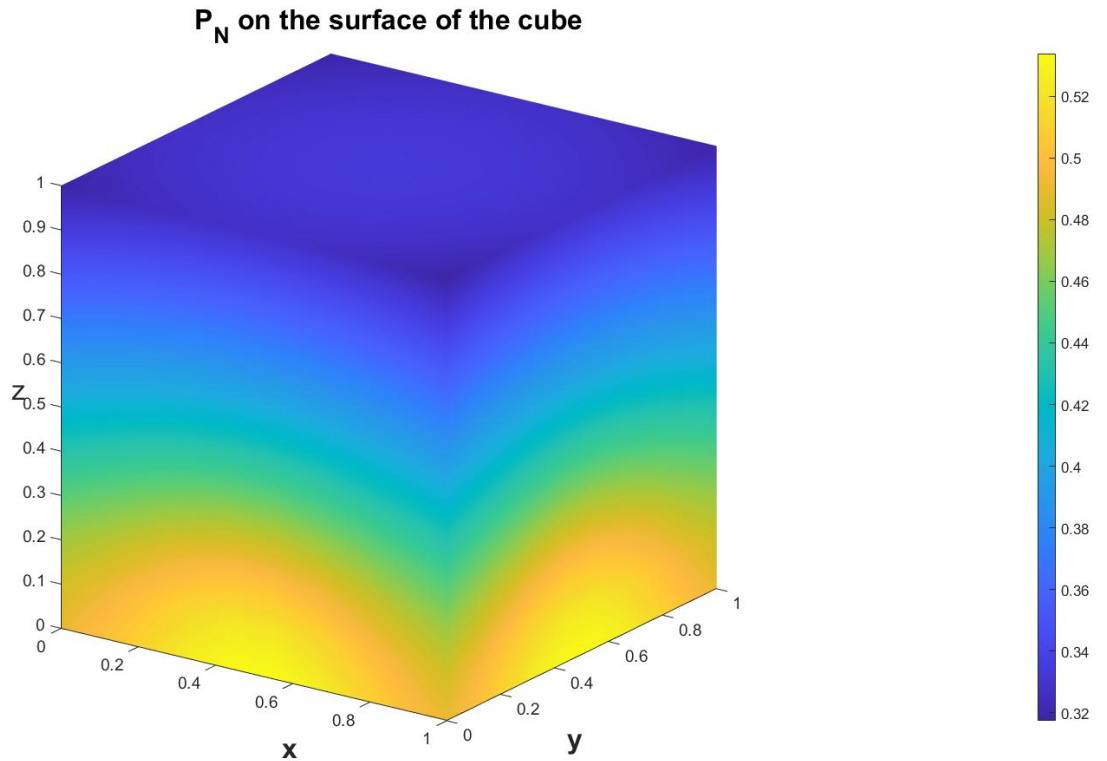


FIGURE 4. The computed approximation  $P_{150}$  of the regular component of the solution.

remaining five faces are grounded. In the absence of free charge, the potential satisfies Laplace's equation with Dirichlet boundary data of the form considered here; see, e.g., [14]. Equivalently, the problem represents the steady-state temperature distribution in a homogeneous cube with no internal heat sources, where the upper face is held at temperature  $T_0$  and the other faces are maintained at zero temperature. The steady temperature then solves Laplace's equation with the same Dirichlet boundary conditions; see, for example, [8].

The S-R method was applied to the above test problem. We computed the values  $\tilde{H}_S(x_i)$  as described in Section 3.4.1. The regular component of the solution was approximated by a harmonic representation in the form of a linear combination of source functions, that is,  $P_N = P_N^H$  with  $N = 150$ . The surface values of  $P_{150}$  are displayed in Figure 4.

With  $P_N$  available, and after computing  $\tilde{H}_S$ , the approximation  $u_N$  takes the form

$$u_N(x) = \tilde{H}_S(x) + P_N(x), \quad x \in \Omega. \quad (4.2)$$

To visualize the singular behavior of the solution, we plot in Figure 5 the solution values along a planar cross-section of the cube near the corner  $(0, 0, 1)$ , where the singularity is most pronounced. The triangular planar section lies at a distance of 0.0866 from the corner, and the solution values  $u$  are visualized using a color-coded representation. The Figure clearly captures the fast singular transition from the value 1 on the upper face to the value 0 on the adjacent faces.

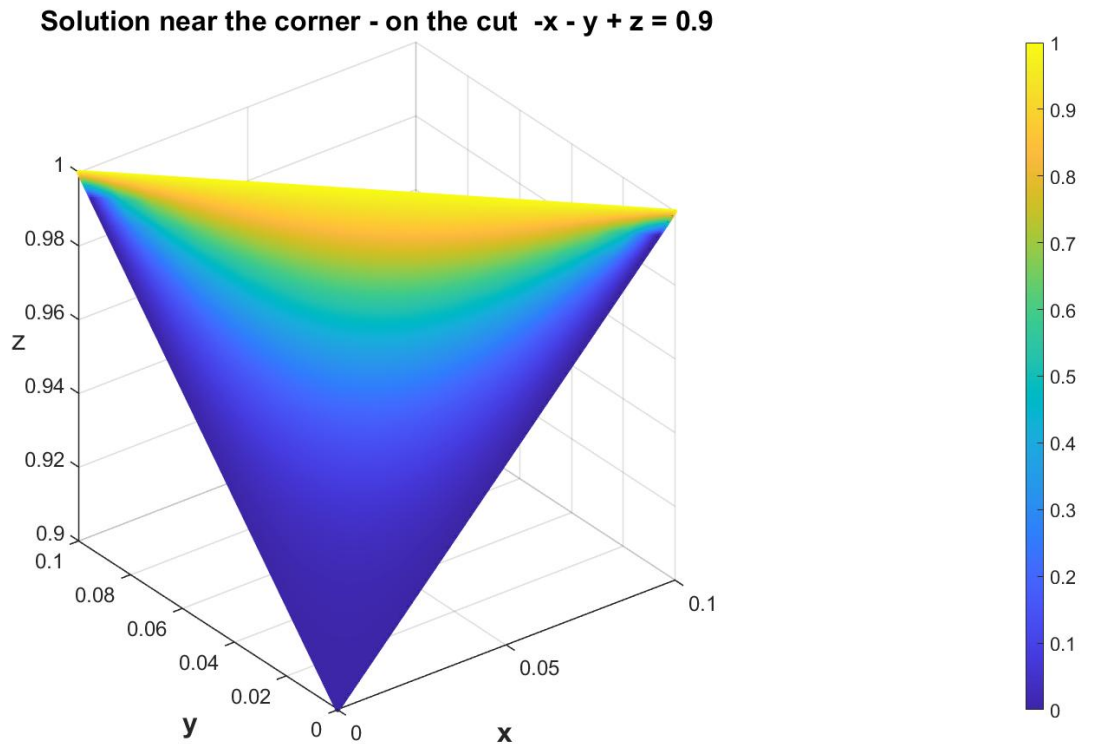


FIGURE 5. The figure displays the computed approximation in the vicinity of the cube corner. It clearly captures the singular transition from the value 1 on the upper face to the value 0 on the adjacent faces.

#### 4.1. The approximation error.

The accuracy of  $u_N$  is affected by three separate sources of error. The first source of error stems from the computation of  $\tilde{H}_S(x_i)$  for  $x_i \in \partial\Omega$ . As discussed in Section 3.4.1, this step reduces to numerically integrating a regular function. Therefore,  $H_S(x_i)$ , and consequently  $H_R(x_i)$ , can be evaluated to any desired accuracy using standard quadrature schemes. The second source of error is associated with the reconstruction of the regular harmonic function from its boundary values. This is discussed in Section 3.4.3. It is shown there that approximation by a linear combination of source functions ( $P_N^{\text{II}}$ , see (3.12)) is stable and provides high accuracy for harmonic functions whose region of regularity is comparable to that of  $H_R$ . As shown in Section 3.13, a reliable estimate  $E_R$  for the approximation error of  $H_R$  throughout the cube can be derived. For the test problem presented above, we obtained the error bound  $E_R^{150} = 0.22 \times 10^{-5}$  for the approximation of  $H_R$ . Increasing the number of interpolation points to

The third source of error arises from the approximation of the surface integrals involved in the computation of  $H_S(x)$ . If  $x$  is sufficiently far from  $\partial\Omega$ , standard tensor-product quadrature rules yield high-order accuracy. When  $x$  is close to  $\partial\Omega$ , we employ tensor-product Simpson quadrature on a rectangular subdivision of the faces, with additional refinement near the near-singular point, as described in Section 3.4.6.

This strategy was employed to generate the results near the corner of the cube shown in Figure 5, using a mesh refinement adapted to the distance of  $x$  from the boundary. The computed values were further validated by additional grid refinement. Overall, a maximum error of  $0.5 \times 10^{-5}$  was achieved for the approximation of  $H_S$  over a uniform distribution of points in the triangular region depicted in Figure 5.

Taking into account the error bound obtained for the approximation of  $H_R$ , and combining it with (3.4) and (4.2), we obtain that over the corner triangle shown in Figure 5 the approximation error satisfies

$$|u(x) - u_{150}(x)| \leq 0.5 \times 10^{-5} + 2.2 \times 10^{-5} = 2.7 \times 10^{-5}. \quad (4.3)$$

## REFERENCES

- [1] Babuška, I.: Finite Element Method for Domains with Corners. *Computing* 6, 264–273 (1970)
- [2] Bacuta, Constantin, Victor Nistor, and Ludmil Zikatanov. "Regularity and well posedness for the Laplace operator on polyhedral domains." arXiv preprint math/0410207 (2004).
- [3] Barnett & Betcke, Stability and convergence of the method of fundamental solutions... , *JCP* 2008
- [4] Bailey, David H., Karthik Jeyabalan, and Xiaoye S. Li. "A comparison of three high-precision quadrature schemes." *Experimental Mathematics* 14.3 (2005): 317-329.
- [5] Canuto, Claudio, et al. Spectral methods: evolution to complex geometries and applications to fluid dynamics. Berlin, Heidelberg: Springer Berlin Heidelberg, 2007.
- [6] Costabel, Martin, Monique Dauge, and Serge Nicaise. "Weighted analytic regularity in polyhedra." *Computers and Mathematics with Applications* 67.4 (2014): 807-817.
- [7] Dai, Feng. Approximation theory and harmonic analysis on spheres and balls. 2013.
- [8] Evans, Lawrence C. Partial differential equations. Vol. 19. American mathematical society, 2022.
- [9] Fairweather, Graeme, and Andreas Karageorghis. "The method of fundamental solutions for elliptic boundary value problems." *Advances in computational mathematics* 9.1 (1998): 69-95.
- [10] Green, George. An essay on the application of mathematical analysis to the theories of electricity and magnetism. author, 1828.
- [11] Grisvard, P.: Elliptic Problems in Nonsmooth Domains. Pitman, Boston, 1985.
- [12] Kozlov, V., Mazya, V., Rossmann, J.: Elliptic boundary value problems in domains with point singularities. Amer. Math. Soc., Providence, RI: 1997.
- [13] Levin, D. "Corrected collocation approximations for the harmonic Dirichlet problem." *IMA Journal of Applied Mathematics* 26.1 (1980): 65-75
- [14] Morse, Philip McCord, and Herman Feshbach. Methods of theoretical physics. Technology Press, 1946.
- [15] Mukhopadhyay, Supratik, and Nayana Majumdar. "A study of three-dimensional edge and corner problems using the neBEM solver." *Engineering Analysis with Boundary Elements* 33.2 (2009): 105-119.
- [16] Ong, E. T., and K. M. Lim. "Three-dimensional singular boundary elements for corner and edge singularities in potential problems." *Engineering Analysis with Boundary Elements* 29.2 (2005): 175-189.

- [17] Walsh, J. L. "The approximation of harmonic functions by harmonic polynomials and by harmonic rational functions." (1929): 499-544.
- [18] Telles, J.C.f. "A self-adaptive co-ordinate transformation for efficient numerical evaluation of general boundary element integrals." International journal for numerical methods in engineering 24.5 (1987): 959-973.